Chapter

Production of Hydroxyapatite on the Surface of Ti6Al7Nb Alloy as Compared to Ti6Al4V Alloy

Elinor Nahum, Svetlana Lugovskoy and Alex Lugovskoy

Abstract

Ti6Al4V is very commonly used for the production of dental implants. Titanium alloys whose mechanical and corrosion properties are equal or better than those of Ti6Al4V might present interest as plausible future materials, too. Ti6Al7Nb alloy was tested and compared to Ti6Al4V in this work. Samples of both alloys were oxidized in a water solution containing calcium acetate ($Ca(CH_3COO)_2$) and calcium glycerophosphate ($Ca(PO_4CH(CH_2OH)_2)$) by Plasma Electrolytic Oxidation (PEO) for 20 min. After that, the samples were hydrothermally treated (HTT) in water (pH = 7) and in potassium hydroxide (KOH) solution (pH = 11) for 2 hours at 200°C in a pressurized reactor. The content and morphology of hydroxyapatite (HA) layers formed on the surface of both alloys after the PEO and subsequent HTT treatments were studied. The surface morphologies, elemental composition, and phase components were characterized by Scanning Electron Microscopy (SEM), Energy Dispersive Spectroscopy (EDS), and X-Ray Diffraction (XRD), respectively. The surface roughness was measured by Atomic Force Microscope (AFM), and thickness measurements were made by SEM and thickness gauge. Corrosion measurements were performed for the comparison of the corrosion behavior of the two alloys.

Keywords: Ti6Al4V, Ti6Al7Nb, plasma electrolytic oxidation (PEO), hydrothermal treatment (HTT), hydroxyapatite (HA)

1. Introduction

Titanium alloys are often used for the production of various tools or devices to be implanted into a human body: artificial joints, blood vessel prostheses, dental implants, and so on. Of the most popular titanium alloys in that field are Ti6Al4V (Titanium grade 5) and Ti6Al4V-ELI (Titanium grade 23), which both have relatively low Young moduli, compatible with that of the bone issues, good fatigue strength, and excellent corrosion resistance in physiological environments [1]. A layer containing mainly Titania (TiO_2) is formed spontaneously on the surface of Titanium alloys. Not only does this layer protect the alloy against corrosion, but it also favors their integration with living tissues, that is, *osseointegration* [2].

Other titanium alloys having suitable properties might present both theoretical and applied interest as the novel materials for medical device production. A Niobium-containing Ti6Al7Nb is one of such alloys. The corrosion behavior of

Ti6Al7Nb in the simulated body fluid (SBF) was studied by Rajendran et al. and was found comparable or better than that of Ti6Al4V-ELI [3].

While the bioinertness (including corrosion stability) of titanium alloys is high enough, their readiness to osseointegration leaves much to be desired [1]. One of the plausible strategies allowing a considerable improvement in the osseointegration of titanium alloys is the production of a layer of Hyfroxyapatite (HA) [4] on their surface. Being a mineral constituent of the bone tissue, Hydroxyapatite is an ideal binder between the metal and the living body.

In this study, the surface modification aiming at the production of HA on the surface of Ti6Al4V and Ti6Al7Nb was made by using Plasma Electrolyte Oxidation (PEO), which is a simple technique for producing hard and rough coating having numerous micro-pores [5, 6]. Using that technique, the insertion into the coating of such elements as calcium and phosphorous may be performed by just adding them to the electrolyte in a suitable form. A PEO layer may also present a diffusional and sorption barrier to the release of metal ions into physiological liquids, thus improving the bioinertness of the core metal [7]. PEO coatings often have good adhesion to the metal even if the implant geometry is complex such as screw-shaped implants [8, 9]. PEO by itself does not cause the growth of HA crystals, rather a specimen needs an additional hydrothermal treatment (HT) [4].

The aim of this study is to compare the efficacy of the production of HA on the surfaces of Ti6Al4V and Ti6Al7Nb by PEO and the subsequent HT.

2. Experimental

Ti6Al4V samples of 40 mm × 20 mm × 1 mm size and Ti6Al7Nb samples of 40 mm × 20 mm × 3 mm size were cut by laser and grounded by 150, 360, 600, and 1000 grid silicon carbide (SiC) papers. The specimens were rinsed in distilled water and acetone in an ultrasonic cleaner for 5 min. The PEO was performed by the 50 Hz sinusoidal AC current in an electrolyte containing 0.25 M calcium acetate and 0.06 M calcium glycerophosphate in distilled water at the current density of 4A/dm^2 for 20 min. The PEO process occurred in a water-cooled stainless-steel container serving as the counter electrode, equipped with a mechanical stirrer. After the completion of the PEO process, the specimens were washed in distilled water and dried on air. After that, the specimens were hydrothermally treated in distilled water or in a KOH solution at 200°C in a pressurized reactor for 2 hours. The pressure during the treatment was 13–15 bar.

The surface morphology and elemental composition were characterized by scanning microscope electron (SEM) TESCAN MAIA3 TriglavTM equipped with AZteq Oxford energy dispersive spectroscopy (EDS) analyzer. X-Ray diffraction (XRD) Rigaku, SmartLab X-RAY DIFRACTOMETER using Cu-Kα radiation (λ = 1.54 Å) in the range of 15–65° angles with a step 0.02° was used to characterize the phase components of the substrates and coating. The thickness of the coatings was measured by ElektroPhysik MiniTest 730 thickness gauge based on eddy current principle by an average of 10 measurements. Focused ion beam (FIB) technique FEI Helios NanoLab™ 600 DualBeam was used for the production of cross-sectional area on a specimen to be further characterized by SEM-EDS. Surface roughness of the samples was evaluated with atomic force microscope (AFM) Bruker's Dimension FastScan with ScanAsystTM using the contact mode.

The corrosion resistance was determined on an IVIUMnSTAT potentiostat by electrochemical polarization methods, namely Linear Polarization Resistance (LPR) and Tafel Slope Extrapolation (TSE) using a three-electrode cell, where an Ag|AgCl electrode served as the reference electrode, and a platinum wire was the counter

electrode. All the corrosion tests were performed in Hank's solution [10] and a simulated saliva solution [11], whose chemical compositions are given in **Table 1**. The pH of the electrolytes was 7, and the temperature was maintained at 36.5°C.

3. Results and discussion

The surface of both titanium alloys after the PEO has the typical for that technique microstructure characterized by microscopic pores scattered randomly across the surface. Cracks seen on the surface are more pronounced for Ti6Al4V (**Figure 1**).

After the hydrothermal treatment, the surface has changed. If the HT is performed in distilled water at pH = 7, Ti6Al4V surface is characterized by grainy HA crystals on the surface and very small needle-like HA crystals inside the pores (**Figure 2a**). Unlike that, numerous HA platelets are observed both inside and outside the pores on the surface of Ti6Al7Nb (**Figure 2b**). If the HT is made at pH = 11, the surface of Ti6Al4V is covered by ununiform plates of significantly larger HA crystals inside and outside the pores (**Figure 2c**). Ti6Al7Nb surface

Hank's solution [10]		**Saliva solution [11]**	
	Composition, g/L	**Reagent**	**Composition, g/L**
$CaCl_2 \cdot 2H_2O$	0.185	$MgCl_2 \cdot 6H_2O$	0.059
$MgSO_4$	0.09767	KCl	0.625
KCl	0.4	KH_2PO_4	0.326
KH_2PO_4	0.06	K_2HPO_4	0.804
$NaHCO_3$	0.35	$CaCl_2 \cdot 2H_2O$	0.166
NaCl	8.0	$C_3H_8O_3$	2.00
Na_2HPO_4	0.04788	Sodium carboxymethyl cellulose	10.0
Glucose	1.0		

Table 1.
Chemical composition of Hank's and simulated saliva solutions.

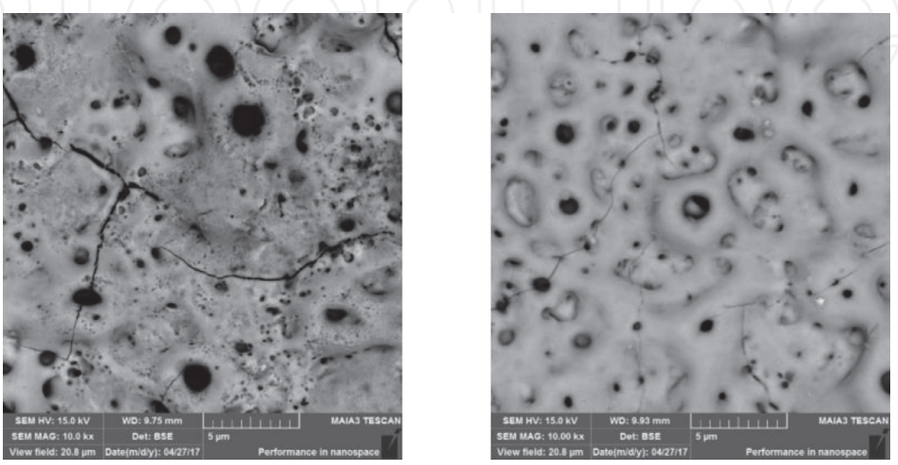

(a) **(b)**

Figure 1.
Back scattered electrons SEM images of the sample's surface after PEO, ×10,000: (a) Ti6Al4V and (b) Ti6Al7Nb.

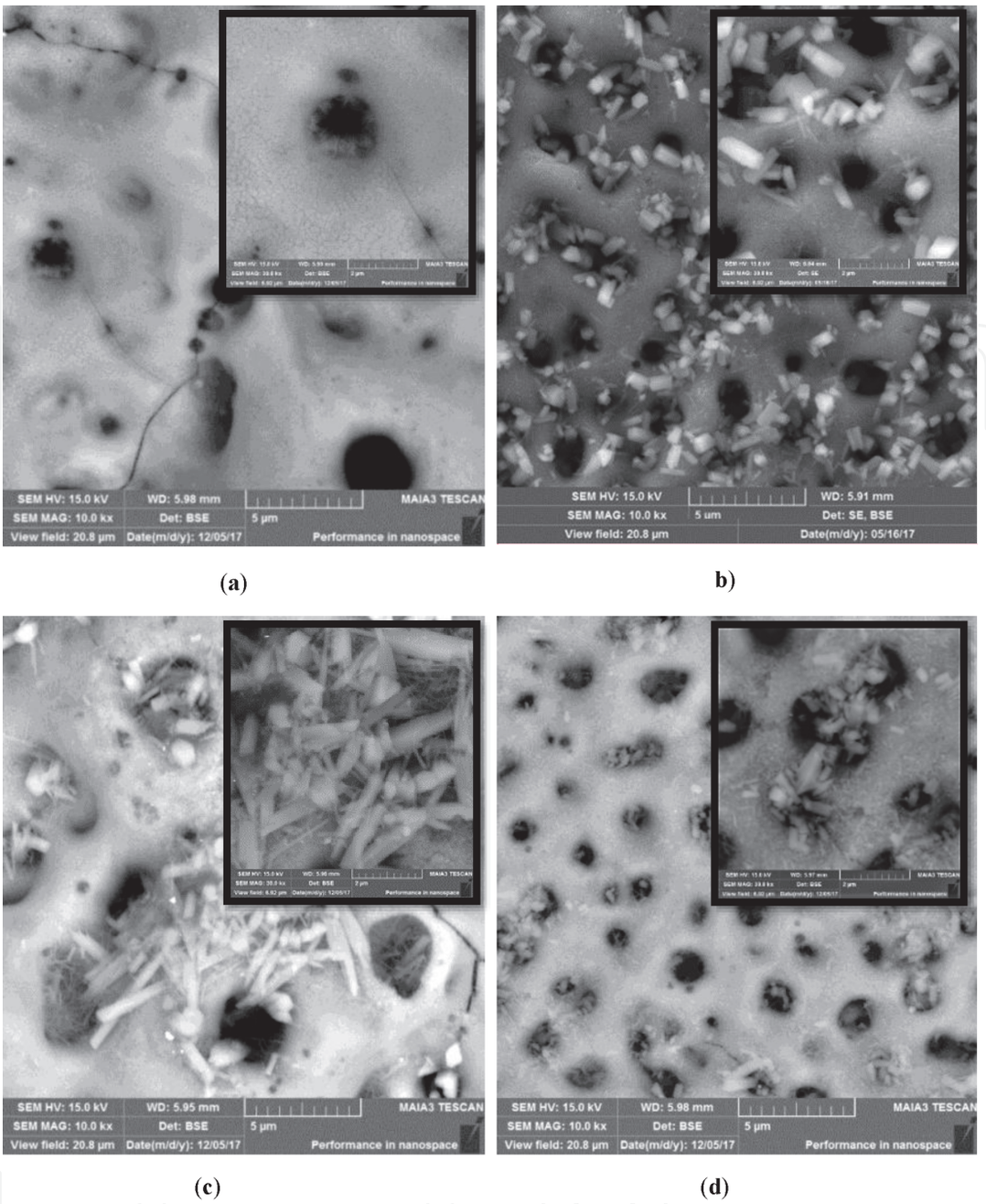

Figure 2.
Surface morphologies after hydrothermal treatment, BSE SEM ×10,000; ×30,000 in the inserts: (a) Ti6Al4V pH = 7; (b) Ti6Al7Nb pH = 7; (c) Ti6Al4V pH = 11; and (d) Ti6Al7Nb pH = 11.

contains large plates of HA inside the pores and a mixture of grainy and needle-like crystals outside the pores (**Figure 2d**).

After the completion of the PEO + HT treatment, the surface layers were partially ablated by FIB, so that the 'cross-sectional' structure could be seen (**Figure 3**). As is seen in **Figure 3**, there is an approximately 1 μm porous PEO oxide layer on the surface of the alloys. The oxide layer has partially amorphous and partially fine crystalline structure (region 'b' in the image); above that, an approximately 1 μm hydroxyapatite layer (region 'c' in the image) consisting of larger crystallites is present. The thicknesses of the oxide and hydroxyapatite layers may vary from one specimen to another, while their structure remains the same.

The elemental compositions of the surfaces obtained by EDS are given in **Table 2**. The presented chemical composition is the average of three-point mode analysis, and standard deviations are displayed. The stoichiometric Ca/P ratio for

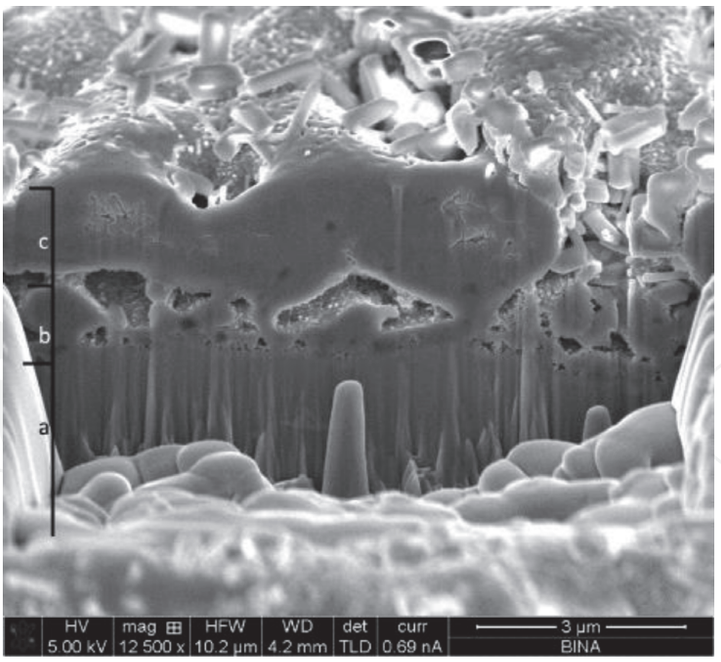

Figure 3.
A typical FIB-ablated cross-sectional structure of the surface: (a) titanium alloy substrate, (b) PEO porous layer, and (c) hydroxyapatite layer.

	Ti	Al	Nb or V	O	Ca	P	Ca/P
Ti6Al4V, PEO	15.1 ± 0.1	1.6 ± 0.0	0.6 ± 0.0	63.3 ± 0.2	8.6 ± 0.0	5.7 ± 0.0	1.51
Ti6Al7Nb, PEO	10.5 ± 0.5	1.2 ± 0.0	0.4 ± 0.0	58.1 ± 0.6	7.5 ± 0.1	4.6 ± 0.0	1.63
Ti6Al4V, HT pH = 7	17.7 ± 1.9	1.9 ± 0.0	3.0 ± 0.2	64.8 ± 0.6	7.2 ± 0.4	4.4 ± 0.2	1.64
Ti6Al7Nb, HT pH = 7	17.9 ± 0.3	2.2 ± 0.1	0.7 ± 0.1	69.8 ± 0.0	5.0 ± 0.3	4.6 ± 0.1	1.09
Ti6Al4V, HT pH = 11	15.5 ± 4.6	1.6 ± 0.7	0.4 ± 0.1	59.9 ± 7.7	11.6 ± 8.5	5.8 ± 3.4	2.00
Ti6Al7Nb, HT pH = 11	14.5 ± 3.4	2.1 ± 0.6	0.6 ± 0.0	65.3 ± 5.3	6.1 ± 3.7	5.1 ± 1.9	1.20

Table 2.
Elemental composition (at%, EDS) of the surfaces after PEO and hydrothermal treatments.

hydroxyapatite is 1.67 that was not observed for any specimen, which means that the surfaces always contain mixtures of various calcium phosphates rather than the pure hydroxyapatite.

In order to determine the phase composition of the surfaces, XRD spectra were measured (**Figure 4** and **Table 3**). It can be seen from **Figure 4** and **Table 3** that for both alloys no detectable amount of HA is present after PEO. Rather, the surfaces are covered by the mixture of rutile and anatase. Additionally, the surface of Ti6Al4V contains a small amount of tricalcium phosphate $Ca_2(PO_4)_2$, which is not the case for Ti6Al7Nb. After the HT treatment, an HA phase is detected on the surface of both alloys.

The thickness of the coating was determined by two different methods (**Table 4**), namely by using a thickness gauge and measuring the FIB-ablated cross sections in SEM images. The measurements reveal higher coating thicknesses for Ti6Al4V than Ti6Al7Nb. Ti6Al4V coating shows also larger and more uneven thickness for Ti6Al4V than for Ti6Al7Nb.

3D AFM images of Ti6Al4V and Ti6Al7Nb after PEO and hydrothermal treatments are shown in **Figure 5**. The area scanned was 5 μm × 5 μm, and three sites were scanned for each specimen. The values of average roughness (R_a) for all the

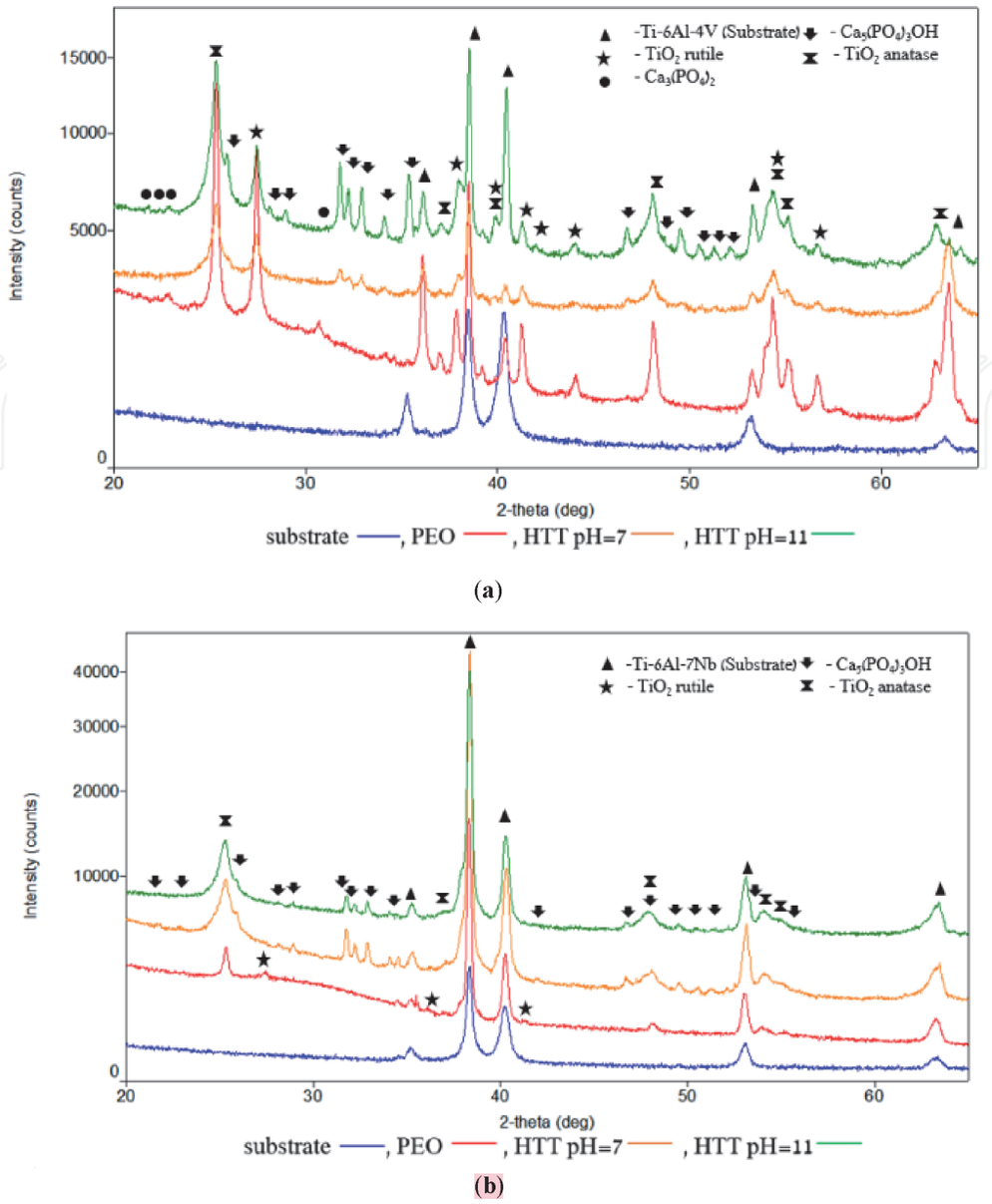

Figure 4.
XRD spectra acquired from the coatings: (a) Ti-6Al-4 V and (b) Ti-6Al-7Nb.

Treatment	Ti6Al7Nb	Ti6Al4V
PEO	TiO_2-rutile, anatase Amorphous phase	TiO_2-rutile, anatase $Ca_3(PO_4)_2$ Amorphous phase
HTT pH = 7	TiO_2-anatase HA	TiO_2-rutile, anatase HA
HTT pH = 11	TiO_2-anatase HA	TiO_2-rutile, anatase HA

Table 3.
Phase composition of coating after PEO and hydrothermal treatments.

specimens lie in the range of 50–250 nm (**Table 5**), and for Ti6Al7Nb, they are higher for all the treatments. As is seen from both AFM (**Figure 5**) and SEM (**Figure 2**) images, a more developed surface with plate-shaped HA crystals inside the pores and grainy crystals on the surface is formed on Ti6Al7Nb than on Ti6Al4V. The roughness range of 10 nm to 10 μm is favorable for the

Ti alloy	Treatment	Average coating thickness by SEM, μm	Average coating thickness by thickness gauge, μm
Ti6Al4V	PEO	6.4 ± 1.2	9.4 ± 1.0
	HTT pH = 7	8.5 ± 1.0	8.8 ± 1.1
	HTT pH = 11	7.0 ± 0.9	9.5 ± 1.2
Ti6Al7Nb	PEO	2.8 ± 0.4	2.8 ± 0.3
	HTT pH = 7	3.2 ± 0.1	2.4 ± 0.2
	HTT pH = 11	3.0 ± 0.6	2.6 ± 0.4

Table 4.
Thickness of the coatings on Ti alloys.

osseointegration because it is compatible with the sizes of small cells and large biomolecules [12, 13].

For the determination of corrosion parameters of the alloys, polarization curves of the specimens in Hank's solution and in artificial saliva were measured in the range of ±250 mV with respect to the OCP at the scan rate of 1 mV/s. Additionally, linear polarization measurements (LPRs) were performed in the narrower range of ±10 mV at the scan rate of 0.5 mV/s. The measured values of corrosion current densities and corrosion potentials are given in **Table 6**. For some cases (these are marked gray in **Table 6**), it was not possible to measure the corrosion parameters because the systems were too passive.

As is seen from **Table 6**, all the corrosion potentials that could be measured are significantly shifted to more noble values after the hydrothermal treatment, so that the alloy is effectively passivated. No essential difference was observed for the corrosion potential of the two alloys (at least, when those were measurable).

The values of corrosion current densities are scattered in a quite random manner and therefore are less informative. We assume that due to the relatively poor electrical conductivity of both liquids (the WC-CE resistance measured in the cell was ~10–20 kΩ for Hank's solution and for the artificial saliva, which is at least by the factor of 1000 higher than for such strong electrolytes as KCl), the precision of the polarization methods was not sufficient.

4. Conclusions

The morphologies, elemental and phase's composition, coating thickness, roughness, and corrosion behavior of Ti6Al4V and Ti6Al7Nb alloys after Plasma Electrolytic Oxidation and the subsequent hydrothermal treatment at various pHs were studied and compared. Hydroxyapatite-containing surfaces can be attained by the two-stage procedure, PEO and HTT, for both alloys.

Thicker, finer, and more uniform oxide layers are formed on the surface of Ti6Al4V than on Ti6Al7Nb for the same treatment parameters.

The most developed surface with plate-shaped HA crystals was obtained for Ti6Al7Nb after HTT in distilled water.

The corrosion potentials are significantly shifted to more noble values after the hydrothermal treatment, so that the alloy is effectively passivated. No essential difference was observed between the corrosion potential of the two alloys. It was

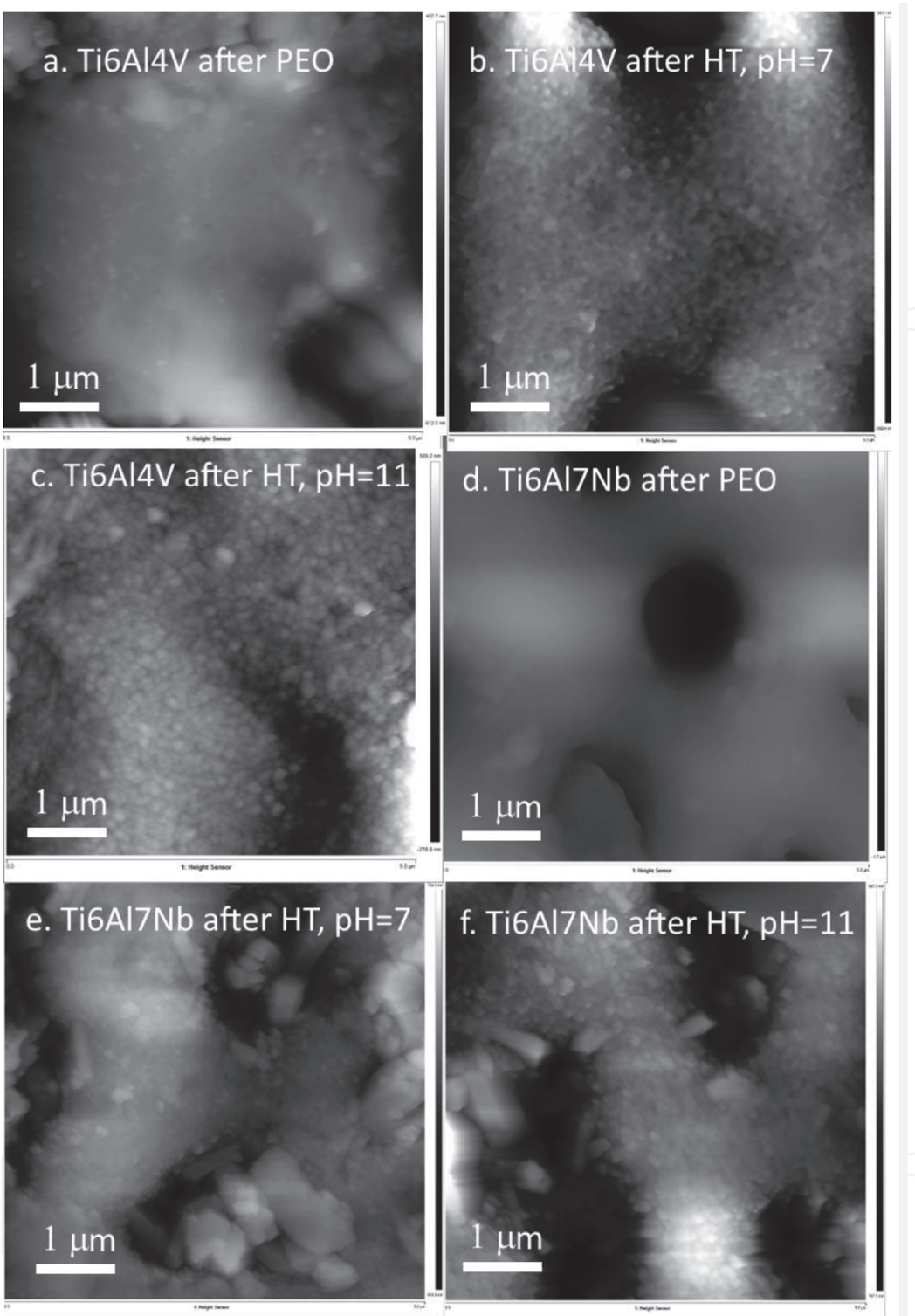

Figure 5.
3D AFM images: (a) Ti6Al4V after PEO; (b) Ti6Al4V after HTT pH = 7; (c) Ti6Al4V after HTT pH = 11; (d) Ti6Al7Nb after PEO; (e) Ti6Al7Nb after HTT pH = 7; (f) Ti6Al7Nb after HTT pH = 11.

	PEO	**HT, pH = 7**	**HT, pH = 11**
Ti6Al4V	83.1	115.7	55.4
Ti6Al7Nb	232.7	175.3	234.7

Table 5.
R_a *values (nm) for Ti6Al4V and Ti6Al7Nb surfaces after PEO and HT treatments.*

		E_{corr}, mV vs. Ag|AgCl	j_{corr}, A/cm^2, LPR	j_{corr}, A/cm^2, Tafel
Ti6Al4V, PEO	Hank's	−293	$3.76 \cdot 10^{-7}$	$2.31 \cdot 10^{-7}$
	Saliva	−303	$2.91 \cdot 10^{-8}$	$2.63 \cdot 10^{-8}$
Ti6Al7Nb, PEO	Hank's	−403	$2.66 \cdot 10^{-6}$	$1.32 \cdot 10^{-6}$
	Saliva		Passive	
Ti6Al4V, HT pH = 7	Hank's	−151	$5.16 \cdot 10^{-7}$	$2.83 \cdot 10^{-7}$
	Saliva	−156	$2.06 \cdot 10^{-7}$	$1.02 \cdot 10^{-7}$
Ti6Al7Nb, HT pH = 7	Hank's		Passive	
	Saliva		Passive	
Ti6Al4V, HT pH = 11	Hank's	−112	$1.38 \cdot 10^{-6}$	$1.23 \cdot 10^{-6}$
	Saliva	−127	$2.32 \cdot 10^{-7}$	$1.30 \cdot 10^{-7}$
Ti6Al7Nb, HT pH = 11	Hank's		Passive	
	Saliva		Passive	

Table 6.
Corrosion current density and corrosion potentials for Ti6Al4V and Ti6Al7Nb in Hank's and saliva solutions.

found that the polarization corrosion measurement is not precise enough for both alloys in Hank's solution and in the artificial saliva because of the poor conductivity of both liquids.

Author details

Elinor Nahum*, Svetlana Lugovskoy and Alex Lugovskoy
Department of Chemical Engineering, Ariel University, Ariel, Israel

*Address all correspondence to: elinorna@ariel.ac.il

References

[1] Manivasagam G, Dhinasekaran D, Rajamanickam A. Biomedical implants: Corrosion and its prevention - A review. Recent Patents on Corrosion Science. 2010;**2**:40-54. DOI: 10.2174/1877610801002010040

[2] Jäger M, Jennissen HP, Dittrich F, Fischer A, Köhling HL. Antimicrobial and osseointegration properties of nanostructured titanium orthopaedic implans. Materials. 2017;**10**:1-28. DOI: 10.3390/ma10111302

[3] Tamilselvi S, Raman V, Rajendran N. Corrosion behaviour of Ti-6Al-7Nb and Ti-6Al-4V ELI alloys in the simulated body fluid solution by electrochemical impedance spectroscopy. Electrochimica Acta. 2006;**52**:839-846. DOI: 10.1016/j.electacta.2006.06.018

[4] Lugovskoy A, Lugovskoy S. Production of hydroxyapatite layers on the plasma electrolytically oxidized surface of titanium alloys. Materials Science and Engineering: C. 2014;**43**: 527-532. DOI: 10.1016/j.msec.2014.07.030

[5] Lugovskoy A, Zinigrad M. Plasma electrolytic oxidation of valve metals. In: Mastai Y, editor. Advances in Materials Science and Engineering. London: InTech; 2013. pp. 85-102. DOI: 10.5772/54827

[6] Ibrahim MZ, Sarhan AAD, Yusuf F, Hamdi M. Biomedical materials and techniques to improve the tribological, mechanical and biomedical properties of orthopedic implants – A review article. Journal of Alloys and Compounds. 2017; **714**:636-667. DOI: 10.1016/j.jallcom.2017.04.231

[7] Mohedano M, Matykina E, Arrabal R, Pardo A, Merino MC. Metal release from ceramic coatings for dental implants. Dental Materials. 2014;**30**:e28-e40. DOI: 10.1016/j.dental.2013.12.011

[8] Zhu X, Chen J, Scheideler L, Reichl R, Geis-Gerstorfer J. Effects of topography and composition of titanium surface oxides on osteoblast responses. Biomaterials. 2004;**25**:4087-4103. DOI: 10.1016/j.biomaterials.2003.11.011

[9] Esen Z, Öcal EB. Surface characteristics and in-vitro behavior of chemically treated bulk Ti6Al7Nb alloys. Surface and Coatings Technology. 2017;**309**:829-839. DOI: 10.1016/j.surfcoat.2016.10.078

[10] Balanced Hank's Solution. Available from: https://www.sigmaaldrich.com/content/dam/sigma-aldrich/docs/Sigma/Formulation/d5796for.pdf

[11] Simulated Saliva Solution. Available from: https://www.pickeringlabs.com/wp-content/uploads/sds/SDS 1700 0305 Artificial Saliva for Medical and Dental Research.pdf

[12] Dilea M, Mazare A, Ionita D, Demetrescu I. Comparison between corrosion behaviour of implant alloys Ti6Al7Nb and Ti6Al4Zr in artificial saliva. Materials and Corrosion. 2013; **64**:493-499. DOI: 10.1002/maco.201206526

[13] Elias CN, Meirelles L. Improving osseointegration of dental implants. Expert Review of Medical Devices. 2010;7:241-256. DOI: 10.1586/erd.09.74